Design of easily synchronizable oscillator networks using the Monte Carlo optimization method

Tatsuo Yanagita*
Research Institute for Electronic Science, Hokkaido University, Sapporo 001-0020, Japan

Alexander S. Mikhailov
Fritz-Haber-Institut der Max-Planck-Gesellschaft, Faradayweg 4-6, 14195 Berlin, Germany
(Received 19 January 2010; published 14 May 2010)

Starting with an initial random network of oscillators with a heterogeneous frequency distribution, its autonomous synchronization ability can be largely improved by appropriately rewiring the links between the elements. Ensembles of synchronization-optimized networks with different connectivities are generated and their statistical properties are studied.

DOI: 10.1103/PhysRevE.81.056204 PACS number(s): 05.45.Xt, 05.10.−a

I. INTRODUCTION

In the last decade, much interest has been attracted to studies of complex networks consisting of dynamical elements involved in a set of interactions [1,2]. Particular attention has been paid to problems of synchronization in network-organized oscillator systems [3,4]. Synchronization phenomena are ubiquitous in various fields of science and play an important role in the functioning of living systems [5]. Investigations focused on understanding the relationship between the topological structure of a network and its collective synchronous behavior [2]. Recently, synchronization properties of systems formed by phase oscillators on static complex networks, such as small-world networks [6] and scale-free networks [7,8], have been considered. It has also been shown that the ability of a network to give rise to synchronous behavior can be greatly enhanced by exploiting the topological structure emerging from the growth processes [9,10]. However, full understanding of how the network topology affects synchronization of specific dynamical units is still an open problem.

One possible approach is to use evolutionary learning mechanisms in order to construct networks with prescribed dynamical properties. Several models have been explored, where dynamical parameters were modified in response to the selection pressure via learning algorithms, in such a way that the system evolved toward a specified goal [11–16]. In our study, this approach is employed to design phase oscillator networks with synchronization properties. We consider adaptive evolution of a network of coupled heterogeneous phase oscillators [17,18]. In such systems, heterogeneity of oscillator frequencies competes with the coupling which favors emergence of coherent dynamics [3,17]. The question is how to connect a set of phase oscillators with given natural frequencies, so that the resulting network would exhibit the strongest synchronization, under the constraint that the total number of available links is fixed.

Previously, a related but different problem of synchronization optimization in a network with the fixed topology through the modification of connection weights was considered [19]. Assuming that the system was in a phase-locked state, the deterministic steepest-descent method was used to determine the coupling strengths between elements which lead to the best possible phase synchronization. In contrast, we consider the systems which stay in partially synchronized states (that is, are not fully phase-locked) and ask what should be the optimal topology of connections, with each link having the same strength.

To design optimal networks, stochastic Markov chain Monte Carlo (MCMC) method with replica exchange is used by us. Large ensembles of optimal networks are constructed and their common statistical properties are analyzed. As we observe, the typical structure of a synchronization-optimized network is strongly dependent on its prescribed connectivity. Sparse optimal networks, with a small number of links, tend to display a structure with relatively high clustering, similar to that found for the networks of chaotic maps [20,21]. As the connectivity is increased, synchronization-optimized networks show a transition to (approximately) bipartite architectures.

The paper is organized as follows. In Sec. II, we present a model of heterogeneous phase oscillators occupying nodes of a directionally coupled network and define the synchronization measure for this system. The optimization method is also presented in this section. Construction of the optimized networks and their statistical analysis are performed in Sec. III. The results are finally discussed in Sec. IV

II. MODEL AND THE OPTIMIZATION METHOD

We consider N oscillators with different natural frequencies placed onto the nodes of a network. The evolution of this system is given by

$$\frac{d\theta_i}{dt} = \omega_i + \frac{\lambda}{N}\sum_{j=1}^{N} a_{i,j}\sin(\theta_j - \theta_i), \tag{1}$$

where ω_i is the natural frequency of oscillator i and λ is the coupling strength. The weights $a_{i,j}$ define the adjacency matrix $\mathbf{a}$ of the interaction network: $a_{i,j}=1$ if oscillator i interacts with oscillator j and $a_{i,j}=0$ otherwise. The adjacency matrix is generally asymmetric.

*yanagita@nsc.es.hokudai.ac.jp; http://www-nsc.es.hokudai.ac.jp/~yanagita

To quantify synchronization of the oscillators, the Kuramoto order parameter

$$r(t) = \frac{1}{N}\left|\sum_{i=1}^{N} \exp(i\theta_i)\right| \tag{2}$$

is employed. Under perfect synchronization, we have $r=1$, whereas $r \sim \mathcal{O}(N^{-1/2})$ in absence of coupling for randomly drawn natural frequencies. A second-order transition takes place at some critical coupling strength λ_c from the desynchronized to the synchronized states [17].

To measure the degree of synchronization, we numerically integrate Eq. (1) for given initial conditions $\theta_i(t=0) \in [0, 2\pi)$ and calculate the average modulus of $r(t)$ over a long time T,

$$R(\mathbf{a}) = \left\langle \frac{1}{T}\int_0^T r(t)dt \right\rangle_{init.}, \tag{3}$$

where $\langle \ldots \rangle_{init.}$ represents an average over many realizations with different initial conditions $\theta_i(0)$.

Our aim is to determine the network $\mathbf{a}$ which would exhibit the highest degree of synchronization, provided that the total number of links is fixed and a set of natural frequencies is given. The network construction can be seen as an optimization problem. The optimization task is to maximize the order parameter and, possibly, bring it to unity by changing the network $\mathbf{a}$. An approximate standard approach to the problems of complex combinatorial optimization, such as the traveling salesman problem, is provided by the method of simulated annealing (see, e.g., [11]). However, we are interested in the *statistical properties* of the synchronization-optimized networks rather than in a search for the best-optimized network. If multiple samples are generated using conventional optimization methods such as simulated annealing, it is difficult to control the probability of the repeated appearance of the same (or similar) items in the obtained set of samples.

To study statistical ensembles of optimized networks, the MCMC method [22–24], which has previously been applied to dynamical systems [25–32], will be used. The canonical ensemble average of a network function $f(\cdot)$ is introduced as

$$\overline{f}_\beta = \sum_w \frac{f(\mathbf{a})\exp[\beta R(\mathbf{a})]}{Z(\beta)}, \tag{4}$$

where $Z(\beta)=\Sigma_w \exp[\beta R(\mathbf{a})]$ is the partition function and the parameter β plays the role of the inverse temperature.

Hence, the problem is reduced to sampling from the ensemble with the Gibbs distribution $\exp[\beta R(\mathbf{a})]$. Such ensemble can be generated, for example, by using the Metropolis algorithm [33], which is the simplest implementation of the MCMC method. The Metropolis algorithm, which we use, is essentially standard. The only important difference is that we should simulate the dynamics with a network $\mathbf{a}$ at each iterated trial.

This Metropolis algorithm appears to provide a simple and universal way of generating the Gibbs network distribution. However, the efficiency of such algorithm gets worse when β increases, particularly in the case of a highly jagged landscape $R(\mathbf{a})$. This deficiency can be eliminated by using instead the replica exchange Monte Carlo (REMC) algorithm, which provides an efficient method to investigate systems with rugged free-energy landscapes, specifically at low temperatures [34–36].

In a REMC simulation, a number of replicas $\{\mathbf{a}_m\}$ with different inverse temperatures β_m are evolved in parallel. At regular evolution time intervals, the performances of a randomly selected, adjacent pair of replicas are compared. The running configurations of the two selected replicas are exchanged with the probability $\min[1, \exp(\Delta\beta\Delta R)]$, where $\Delta\beta=\beta_{m+1}-\beta_m$ is the difference of the inverse temperatures of the pair and $\Delta R=R(\mathbf{a}_{m+1})-R(\mathbf{a}_m)$ is the difference of their performances. The exchange of replicas with different temperatures effectively imitates repeated heating and annealing, thus preventing trapping in the local performance optima. Note that such stochastic exchange algorithm preserves the joint probability distribution $\Pi_m \exp[\beta_m R(\mathbf{a}_m)]/Z(\beta_m)$, so that the unbiased set of samples is generated for all inverse temperatures.

Explicitly, the algorithm is defined as follows:

(1) The states of replicas $\{\mathbf{a}_m^0\}$ are initialized by random networks (which is chosen as a random Erdös-Rényi network).

(2) The candidate for the next network $\mathbf{a}'_m$ at iteration step n is obtained from the current network $\mathbf{a}_m^{(n)}$ by rewiring one of its links. A randomly chosen link is moved to a randomly chosen link vacancy, so that the total number of links remains conserved.

(3) The evolution equations (1) for the network $\mathbf{a}'_m$ are integrated using the standard Euler algorithm. The order parameter is then calculated and averaged over the time interval $t \in [0, T]$ and over a fixed number of realizations starting from different random initial conditions. Thus, the synchronization property $R(\mathbf{a}'_m)$ of the candidate network is determined.

(4) Next, a random number $x \in [0, 1]$ is uniformly drawn. If

$$x < \frac{\exp[\beta R(\mathbf{a}'_m)]}{\exp[\beta R(\mathbf{a}_m^{(n)})]},$$

the candidate is accepted and taken as $\mathbf{a}_m^{(n+1)}=\mathbf{a}'_m$; otherwise nothing is changed, so that $\mathbf{a}^{(n+1)}=\mathbf{a}_m^{(n)}$.

(5) At regular evolution time intervals, the performances of a randomly selected, adjacent pair of replicas are compared. The running configurations of the two selected replicas are exchanged with the probability

$$\min[1, \exp\{(\beta_{m+1}-\beta_m)\{R[\mathbf{a}_{m+1}^{(n+1)}]-R[\mathbf{a}_m^{(n+1)}]\}\}].$$

(6) Return to step (2) until the statistical average Eq. (4) converges.

III. NUMERICAL ANALYSIS

To determine the synchronization degree of a given network at each iteration step of the optimization procedure, Eq. (1) was numerically integrated with the time increment $\Delta t = 0.05$. Averaging over five independent realizations started

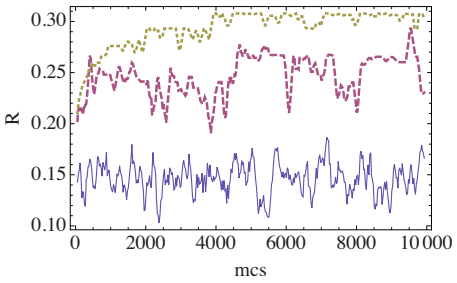

FIG. 1. (Color online) Evolution of order parameters of coupled oscillator networks during the optimization process. Blue solid, red broken, and yellow dotted lines are for $\beta=\beta_0$, β_5, and β_M, respectively. Note that the blue solid line is for $\beta_0=0$ and, therefore, it corresponds to the networks generated by only random rewiring. The parameters are $p=0.2$, $N=20$, $\lambda=1.0$, $\gamma=0.3$, $M=21$, $\delta\beta=10$.

from different random initial conditions has been furthermore performed at each iteration step. Oscillator ensembles of sizes $N=10$ and 20 were considered. Natural frequencies of the oscillators were always chosen as $\omega_i=-\gamma+2\gamma i/N$, so that they uniformly distributed within the interval $[-\gamma,\gamma]$ [40].

Initial phases $\theta_i(0)=2\pi f_{init}(i)/N$ uniformly distributed inside the interval $[0,2\pi)$, where $f_{init}(i)$ is a random one-to-one mapping between $\{1,\ldots,N\}$. Hence, the order parameter at $t=0$ always zero. To construct initial random networks with a given number K of connections and, thus, the connectivity $p=K/N(N-1)$, K off-diagonal elements of the adjacency matrix were randomly and independently selected and set equal to unity.

For time averaging, intervals of length $T=100$ and 200 were typically used. The results did not significantly depend on T when sufficiently large lengths T were taken. Using the order parameter, graphs **a** were sampled by the REMC optimization method. In parallel, evolution of M replicas with the inverse temperatures $\beta_m=\delta\beta m$, $m=0,1,\ldots,M$ was performed (with $M=21$ and $\delta\beta=10$). At each five Monte Carlo steps (mcs), the performances of a randomly chosen pair of replicas were compared and exchanged, as described above. For display and statistical analysis, sampling at each every 50 mcs after a transient of 5000 mcs has been undertaken.

A. Optimization at different temperatures

Synchronization-optimized networks were obtained by running the evolutionary optimization. In this process, the order parameter was progressively increasing until a stationary state has been achieved. Figure 1 displays the optimization processes at different temperatures. As clearly seen, when using replicas with the larger inverse temperature β, the larger values of the order parameter could be reached, although the optimization process was then slower. After the transients, statistical averaging of the order parameter over the ensemble with the Gibbs distribution has been performed, according to Eq. (4).

In Fig. 2(a), the averaged order parameter $\bar{R}$ is displayed as a function of the connectivity p for several different inverse temperature β. The blue solid circle symbols show the averaged order parameter corresponding to the replica with $\beta_0=0$, i.e., for an infinitely high temperature. We see that the averaged order parameter increases with the network connectivity p even if the networks are produced by only random rewiring. The red open circles show the average order parameters for the ensemble corresponding to the replicas with the lowest inverse temperature β_M. Generally, greater order parameters are obtained by running evolution at higher inverse temperatures β at any network connectivity p. At each connectivity p, the order parameter is gradually increased with increasing β and is approximately saturated at β_M. This means that, even if one further increases β, only slight improvements of the averaged order parameter can be expected. Thus, the networks sampled by the replica with the largest inverse temperature β_M are already yielding a representative optimal ensemble.

Figure 2(b) shows, depending on the network connectivity p, the ratio $\overline{R_{\beta_M}}/\overline{R_{\beta_0}}$ of the averaged order parameters sampled by the optimal network ensemble with β_M to those obtained for the ensemble with purely random rewiring. Since there is no room for the improvement of the order parameter when the number of links is small, the ratio tends to unity as the connectivity p is decreased. On the other hand, when $p=1$, global coupling is realized, for which, under the chosen coupling strength, full synchronization occurs. As evidenced by this figure, the difference between the synchronization capacities of the optimized and random networks is most pronounced at the intermediate connectivities p.

In Fig. 2(c), the mean variance $\overline{\mathrm{Var}[R]}_\beta=\overline{R_\beta^2}-\overline{R_\beta}^2$ of the order parameters at different connectivities p is displayed. It can be observed that this mean variance for the synchronization-optimized ensemble decreases with an increase in the number of links, while the respective mean

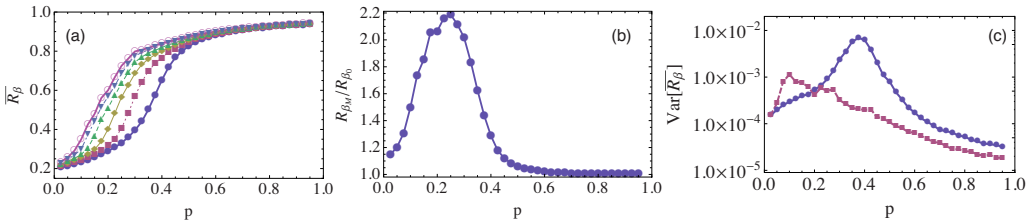

FIG. 2. (Color online) Average order parameters as functions of the network connectivity p. Blue filled circles are for the replica β_0, i.e., the ensemble of randomly rewired networks. Red squares, yellow diamonds, green triangles, blue inverted triangles, and red open circles are for replicas with $\beta=40$, 80, 120, 160, and 200, respectively. (b) Ratio of the average order parameters for the synchronization-optimized ensemble with the inverse temperature β_M and for $\beta_0=0$. (c) Variance of the order parameters. Red squares are for the random rewired ensemble and blue circles are for the synchronization-optimized ensemble. The same parameters as in Fig. 1

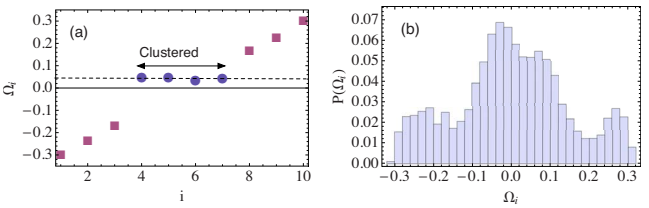

FIG. 3. (Color online) (a) Time-averaged frequencies (winding numbers) of the oscillators in a synchronization-optimized network. (b) Statistical distribution of winding numbers for the synchronization-optimized ensemble. The parameters are $p=0.2$, $\beta=\beta_M$; others are the same as in Fig. 1.

variance for the random rewired ensemble has a maximum at $p=0.4$. Note that, since the transition from the connected to the disconnected random graphs occurs at $p_c=1/N$ [1,2], this behavior is not directly related to the topological transition in the network itself.

To further analyze the behavior of oscillators in synchronization-optimized networks, we calculated time-averaged frequencies, i.e., winding numbers $\Omega_i=(1/T)\int_0^T\theta_i(t)dt$ of all oscillators i. Histograms of distributions over the winding numbers were constructed by counting the numbers of oscillators with the winding number inside a fixed bin interval, $H_k=\{\Omega_i|n\delta\Omega<\Omega_i<(k+1)\delta\Omega\}$, where $k=0,1,\ldots,K-1$, $K=10$ is the number of bins, and $\delta\Omega=2\gamma/K$ is the bin size. The winding number as a function of the natural frequency is shown in Fig. 3(a). The blue circles show the entrained cluster with the winding number approximately equal to zero. The cluster consists of the elements whose natural frequencies are near the mean natural frequency $\Omega=0$. While the specific elements of the cluster and its size depend on a particular network in the synchronization-optimized ensemble, there is a statistical trend that the entrained cluster consists of the oscillators in the neighborhood of the zero frequency. This is demonstrated by the histogram of winding numbers for the synchronization-optimized ensemble in Fig. 3(b). Note that the oscillators are always ordered according to their natural frequencies $\omega_i=-\gamma+2\gamma i/N$ which monotonously increase with i. We see that all elements get divided into two groups, in which $\Omega_i\approx 0$ or where the winding number is relatively high. For each particular network realization, there should be a peak at the frequency of the entrained cluster. The position of this peak depends however on the realization and, as a result, the histogram of the winding numbers for the entire ensemble shows a broad maximum. This behavior is characteristic for relatively low connectivities. The broad peak gradually sharpens when the connectivity is increased because the size of the cluster increases and fluctuations of the winding number become smaller.

B. Architectures of synchronization-optimized networks

Typical structures of synchronization-optimized networks are shown in Fig. 4. When the connectivity p is small, such networks usually represent chain fragments. At a higher connectivity, the network becomes more complexly organized, as shown in Fig. 4(b).

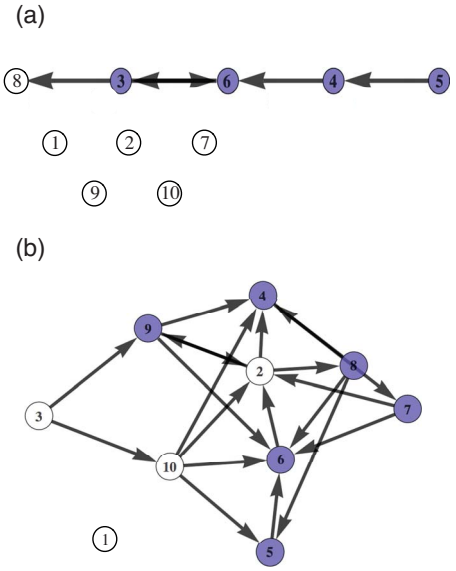

FIG. 4. (Color online) Two typical realizations of the synchronization-optimized network at different connectivities (a) $p=0.05$ and (b) $p=0.2$. Blue (gray) nodes indicate entrained oscillators. Numbers in the nodes are indexes of the oscillators. Parameters are $N=10$, $\beta=\beta_M$, $M=11$, and $\delta\beta=10$.

To statistically characterize the architecture of constructed networks, ensemble averages of their adjacency matrices over the Gibbs ensemble, i.e.,

$$\overline{\mathbf{a}}_\beta=\sum_{\mathbf{a}}\mathbf{a}\exp[\beta R(\mathbf{a})]/Z(\beta), \tag{5}$$

for different connectivities p were computed for $\beta=\beta_M$, as shown in Fig. 5. Clearly, the optimal network structure is changing with the number of links. When the number of links is small, the elements of the mean adjacency matrix, obtained by averaging over many realization from the synchronization-optimized ensemble, are large near the diagonal. Hence, elements with close natural frequency tend to connect and form a chain fragment. Moreover, oscillators with the natural frequencies near the center of the interval are often connected. Increasing the number of links, the network becomes more complicated and off-diagonal elements begin to dominate instead. The network with the larger p tends to have interlaced structures, seen in Figs. 5(b) and 5(c), where the oscillators with roughly opposite natural frequencies are coupled. A similar trend toward anticorrelations for the oscillators with opposite frequencies has been noticed in [15,16], where a transition from local to global synchronization under an increase of the coupling strength has been obtained using a different optimization method [16].

This structural transition can be understood as follows. When connectivity is small, a limited small number of available links is better used to connect oscillators with frequencies in the middle of the frequency interval, where the collective synchronization frequency would lie. Indeed, such oscillators can be easily entrained and even a single link may be sufficient to synchronize them. If connectivity is increased and some further links may be used, it would not however be

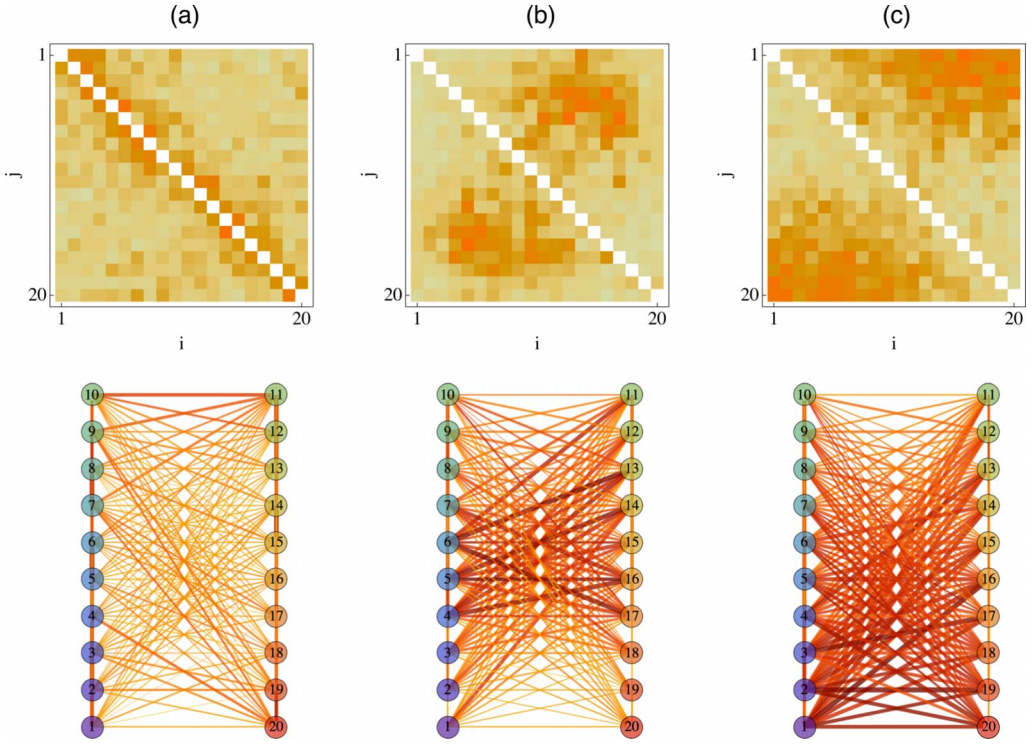

FIG. 5. (Color online) Upper panels show adjacent matrices averaged over the Gibbs ensemble of synchronization-optimized networks [see Eq. (5)]. Darker color of a matrix element indicates the higher probability of the respective connections between the elements. Lower panels display the corresponding network averaged over the Gibbs ensemble. Numbers in the circles show indexes of the oscillators. The thickness of the lines connecting the nodes is proportional to the frequency of links between them. The network connectivities are (a) $p=0.05$, (b) 0.2, and (c) 0.3. Other parameters are same as in Fig. 1.

efficient to put them into the middle region: the oscillators there are already synchronized and bringing more connections would not increase the performance. This means that the additional available links should be rather connected to the elements in the periphery, outside of the central frequency region. If predominantly local connections between the elements on each side are established, this would however lead to the formation of two clusters, each on a different side from the center. Within each cluster, oscillators may get synchronized, but oscillations of the two clusters will still then be incoherent. Therefore, a better solution would consist in establishing pairwise connections between the elements on both sides of the center, i.e., in linking preferentially the opposite oscillators. This is exactly what we observe in Fig. 5 at the higher connectivity $p=0.3$.

C. Degree distributions and cluster organization

To statistically investigate architectures of designed networks, ingoing and outgoing degrees of their nodes have been considered and averaged over the ensemble. Since the network is colored, i.e., each of its node has a different natural frequency, the mean in-degree and out-degree of the nodes can be plotted as a function of their natural frequency (Fig. 6). When connectivity p is small, both in-degree and out-degree averaged over the ensemble have a maximum at $\omega=0$, i.e., oscillators having smaller magnitudes of the natural frequency tend to be mutually connected. This unimodal degree distribution is consistent with the linear-chain structure shown in Fig. 5(a). As p is increased, the mean in-degree distribution becomes bimodal and oscillators having larger magnitudes of the natural frequency tend to have larger out-

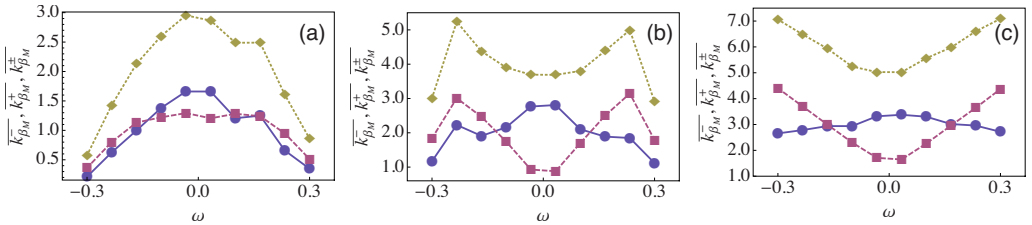

FIG. 6. (Color online) Degrees, averaged over the Gibbs ensemble of synchronitaion-optimized networks, as functions of the natural frequency of the oscillator. The in-degree $\overline{k^-_{\beta_M}}$, out-degree $\overline{k^+_{\beta_M}}$, and degree $\overline{k^\pm_{\beta_M}}$ are plotted by the blue circles, red squares, and yellow diamonds. $N=10$, $\beta=\beta_M$. The network connectivities are (a) $p=0.1$, (b) $p=0.2$, and (c) $p=0.3$. Other parameters the same as in Fig. 1.

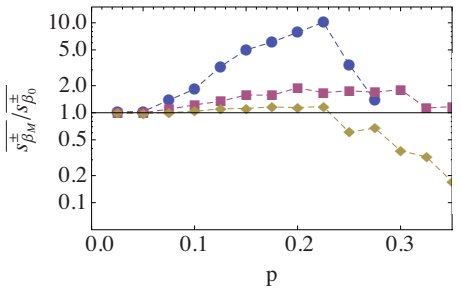

FIG. 7. (Color online) Ratio of the number of isolated nodes, averaged over the replicas with β_M (synchronization-optimized networks) to that averaged over the replicas with β_0 (randomly rewired networks) as a function of the connectivity p. Data for the nodes isolated with respect to incoming (blue circles) and outgoing (red squares) connections, as well as for the completely isolated nodes (yellow diamonds), are shown. The same parameters as in Fig. 1.

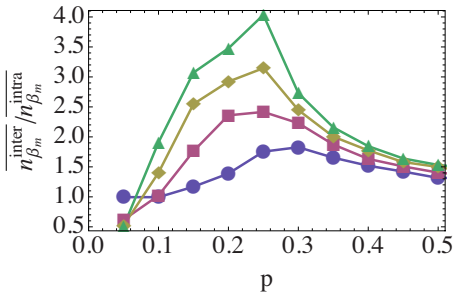

FIG. 8. (Color online) Ratio of interconnections to intraconnections as a function of the connectivity p for $\beta=\beta_5$ (blue circles), β_{10} (red squares), β_{15} (yellow diamonds), and β_{20} (green triangles). $N=10$. The same other parameters as in Fig. 1.

degrees. This tendency becomes stronger when p increases [Figs. 6(b) and 6(c)].

Furthermore, we calculated the mean numbers of isolated nodes as a function of p. The isolated nodes have been classified into three categories, as those which have no in-coming, no out-going, and neither in-coming nor out-going connections. The numbers of such isolated nodes are, respectively,

$$s^{+}(\mathbf{a}) = \sum_{i=1}^{N} \Delta\left(\sum_{j=1}^{N} a_{i,j}\right),$$

$$s^{-}(\mathbf{a}) = \sum_{j=1}^{N} \Delta\left(\sum_{i=1}^{N} a_{i,j}\right),$$

$$s^{\pm}(\mathbf{a}) = \sum_{k=1}^{N} \Delta\left(\sum_{i=1}^{N} a_{i,k} + \sum_{j=1}^{N} a_{k,j}\right), \tag{6}$$

where $\Delta(w)$ is the Kronecker symbol, $\Delta(w)=1$ for $w=1$, and $\Delta(w)=0$ otherwise. We averaged these numbers over the Gibbs ensemble for $\beta=\beta_0$ and β_M and determined the ratio $\overline{s^{\pm}_{\beta_M}}/\overline{s^{\pm}_{\beta_0}}$ of the average number of isolated nodes in the synchronization-optimized networks to that in the networks obtained by random rewiring (see Fig. 7).

The results do not depend on the choice of β_m qualitatively. When p is small, the ratio of completely isolated nodes is larger than 1. This comes from the fact that the links are used intensively between the nodes having smaller magnitudes of the natural frequency at the cost of connections of periphery oscillators. Thus, the number of isolated nodes is large. Starting from $p \simeq 0.23$, this ratio becomes however less than 1, so that the optimized networks tend to have less completely isolated nodes as their random counterparts. We can also notice that the relative number of nodes without ingoing connections becomes high at about $p \simeq 0.23$ and then sharply drops down. The number of nodes without the outgoing connections in the optimized networks remains always larger than in the random networks.

As already suggested by Figs. 5(b) and 5(c), synchronization-optimized network with larger connectivities may be similar to bipartite graphs. A bipartite graph is a graph whose nodes can be divided into two disjoint sets A and B, so that every link connects a node in A to a node in B and *vise versa* [37]. To demonstrate that our optimized networks are indeed similar to bipartite graphs, we divide all oscillators into two groups A and B with the negative and positive natural frequencies. An intraconnection is defined as a link between nodes belonging to the same group, while an interconnection is a link between the nodes in A and B. Thus, the number of intraconnections is given by

$$n^{intra}(\mathbf{a}) = \left(\sum_{i=1,\ j=N/2}^{N/2,N} + \sum_{i=N/2,\ j=1}^{N,N/2}\right) a_{i,j}$$

and the number of interconnections is

$$n^{inter}(\mathbf{a}) = \left(\sum_{i=1,\ j=1}^{N/2,N/2} + \sum_{i=N/2,\ j=N/2}^{N,N}\right) a_{i,j}.$$

The mean ratio $\overline{n^{inter}_{\beta_m}}/\overline{n^{intra}_{\beta_m}}$ of interconnections to intraconnections in the synchrony-optimized ensemble for β_5, β_{10}, β_{15}, and β_{20} as a function of the connectivity p is shown in Fig. 8. This ratio is smaller than unity when connectivity p is small. It increases with p and reaches a maximum in the vicinity of the transition point, where the bipartitelike structure emerges. Further above the transition point, the ratio gradually decreases to unity, since the number of links increases until all-to-all connections are established [41].

D. Closeness, betweenness, and clustering

To characterize network structure quantitatively, we calculated the closeness, betweenness, and clustering coefficient [2,38]. Again, averaging was performed over many realizations of synchronization-optimized networks, sampled with the Gibbs distribution [Eq. (4)].

The betweenness centrality of a node is the number of geodesics (i.e., shortest paths) going through it. If there is more than one geodesic between two nodes, the number of geodesics which connect these two nodes via a considered node is divided by the total number of geodesics that connect the two nodes. The betweenness centrality is thus defined by

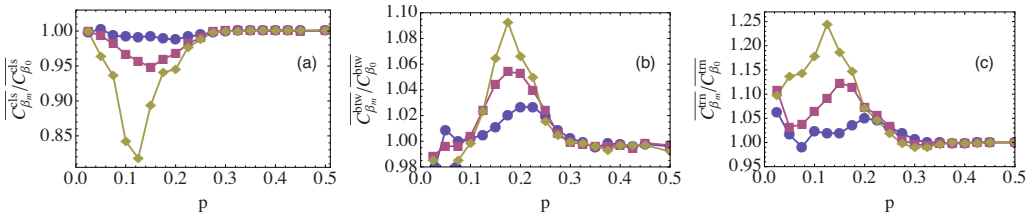

FIG. 9. (Color online). Statistical properties of synchronization-optimized networks as functions of the connectively p. (a) The ratio of closeness, averaged over the replicas with β_m to that averaged over the replicas with β_0, (b) the ratio of betweenness, and (c) the ratio of transitivity, for different β_m, where $m=10$ (blue circles), $m=15$ (red squares), and $m=20$ (yellow diamonds). The same parameters as in Fig. 1.

$$C^{btw}(v) = \sum_{s,t} \sum_{s \neq t} \frac{\sigma_{s,t}(v)}{\sigma_{s,t}},$$

where σ is the number of shortest paths from node s to node t and $\sigma_{s,t}(v)$ is the number of shortest paths from s to t that pass through node v.

The closeness centrality of a node specifies how easily other nodes can be reached from it (or, in other words, how easily it can be reached from the other nodes). It is defined as the sum of the lengths of all geodesics leading to or from the given node, divided by the total number n of nodes minus 1

$$C^{cls}(v) = \frac{1}{n-1} \sum_{t} d_g(v,t),$$

where $d_g(u,v)$ is geodesic distance between the nodes u and v (i.e., the length of the shortest path connecting them).

The clustering coefficient of a node specifies the number of neighbors of this node which are in turn mutual neighbors. It is defined as

$$C^{trn}(v) = \frac{t_v}{c_2^{k_v}},$$

where k_v is the degree of a node v, t_v is the number of links between its neighbors, and $c_2^{k_v}$ is the number of pairs that can be made by using k_v neighbors.

The above properties are defined for each node. To characterize the entire network, we average them over all nodes. In order to quantify differences between synchronization-optimized networks and networks generated by random rewiring, ratios $\overline{C^K(\mathbf{a})}_{\beta_m} / \overline{C^K(\mathbf{a})}_{\beta_0}$ can be used, where C^K is the respective property of network, such as closeness, betweenness, or clustering, β_m is inverse temperature, and $\beta_0=0$. In Fig. 9, we show these ensemble-averaged network properties depending on the connection probability p for several inverse temperatures. Obviously, these ratios should approach unity at $p=0$ or at $p=1$ because the difference in synchronization of optimized and random networks vanishes in these two limits. The ratios for the closeness have pronounced minima in the transition region. The ratio in the vicinity of the transition point decreases when the performance of optimized network increases, i.e., the network ensemble with higher inverse temperature.

On the other hand, the betweenness and clustering coefficient gradually increase with the connectivity p and reach a maximum in the transition region. Note that in recent work [39], it was found that, both in random and scale-free networks, increase the clustering coefficient favors formation of oscillator subpopulations synchronized at different frequencies.

IV. CONCLUSIONS

We have designed synchronization-optimized networks with a fixed number of links for a heterogeneous oscillator population. This has been done by using the Markov chain stochastic Monte Carlo method complemented by the replica exchange algorithm. A transition from the linear to bipartite-like networks has been found under increasing the number of links. At low connectivity, synchronization-optimized networks typically represent small chains connecting oscillators with close natural frequencies. As the number of links increases, the networks become interlaced and oscillators with opposite natural frequencies tend to be connected. Therefore, synchronization-optimized network begin to resemble bipartite graphs. This structural change of synchronion-optimized network is clearly revealed through the analysis of interconnections and intraconnections.

Thus, we have shown that the efficient design of oscillator networks with the improved synchronization properties is possible. The architectures of such optimal networks strongly depend on the constraints, such as the total number of links available. Through the appropriate rewiring of a network, a strong gain in the synchronization signal can be achieved.

Although our study has been performed for a simple system of phase oscillators, similar evolutionary optimization methods can be applied to construct networks of different origins, where the dynamics of individual oscillators may be significantly more complex.

ACKNOWLEDGMENTS

This study has been partially supported by the Ministry of Education, Science, Sports and Culture, Grant-in-Aid for Scientific Research (Grant No. 21540376) and the Volkswagen Foundation (Germany).

[1] R. Albert and A.-L. Barabási, Rev. Mod. Phys. **74**, 47 (2002).
[2] S. Boccaletti, V. Latora, Y. Moreno, M. Chavez, and D.-U. Hwang, Phys. Rep. **424**, 175 (2006).
[3] S. Manrubia, A. Mikhailov, and D. Zanette, *Emergence of Dynamical Order: Synchronization Phenomena in Complex Systems* (World Scientific, Singapore, 2004).
[4] A. Arenas, A. Diaz-Guilera, J. Kurths, Y. Moreno, and C. Zhou, Phys. Rep. **469**, 93 (2008).
[5] J. Kurths, A. Pikovsky, and M. Rosenblum, *Synchronization: A Universal Concept in Nonlinear Sciences* (Cambridge University Press, Cambridge, England, 2001).
[6] H. Hong, M. Y. Choi, and B. J. Kim, Phys. Rev. E **65**, 026139 (2002).
[7] T. Ichinomiya, Phys. Rev. E **70**, 026116 (2004).
[8] D.-S. Lee, Phys. Rev. E **72**, 026208 (2005).
[9] A. E. Motter, C. Zhou, and J. Kurths, Phys. Rev. E **71**, 016116 (2005).
[10] D.-U. Hwang, M. Chavez, A. Amann, and S. Boccaletti, Phys. Rev. Lett. **94**, 138701 (2005).
[11] M. Ipsen and A. S. Mikhailov, Phys. Rev. E **66**, 046109 (2002).
[12] L. G. Moyano, G. Abramson, and D. H. Zanette, Eur. Phys. J. B **22**, 223 (2001).
[13] P. M. Gleiser and D. H. Zanette, Eur. Phys. J. B **53**, 233 (2006).
[14] L. Buzna, S. Lozano, and A. Díaz-Guilera, Phys. Rev. E **80**, 066120 (2009).
[15] M. Brede, Phys. Lett. A **372**, 5305 (2008).
[16] M. Brede, Eur. Phys. J. B **62**, 87 (2008).
[17] Y. Kuramoto, *Chemical Oscillations, Waves, and Turbulence* (Springer, New York, 1984).
[18] J. A. Acebrón, L. L. Bonilla, C. J. Pérez Vicente, F. Ritort, and R. Spigler, Rev. Mod. Phys. **77**, 137 (2005).
[19] T. Tanaka and T. Aoyagi, Phys. Rev. E **78**, 046210 (2008).
[20] P. Gong and C. van Leeuwen, Europhys. Lett. **67**, 328 (2004).
[21] D. van den Berg and C. van Leeuwen, Europhys. Lett. **65**, 459 (2004).
[22] D. Landau and K. Binder, *A Guide to Monte Carlo Simulations in Statistical Physics* (Cambridge University Press, London, 2005).
[23] M. E. J. Newman and G. T. Barkema, *Monte Carlo Methods in Statistical Physics* (Oxford University Press, New York, 1999).
[24] J. Liu, *Monte Carlo Strategies in Scientific Computing* (Springer, New York, 2001).
[25] A. E. Cho, J. D. Doll, and D. L. Freeman, Chem. Phys. Lett. **229**, 218 (1994).
[26] P. G. Bolhuis, C. Dellago, and D. Chandler, Faraday Discuss. **110**, 421 (1998).
[27] T. Vlugt and B. Smit, PhysChemComm. **2**, 11 (2000).
[28] M. Kawasaki and S. I. Sasa, Phys. Rev. E **72**, 037202 (2005).
[29] S. I. Sasa and K. Hayashi, Europhys. Lett. **74**, 156 (2006).
[30] C. Giardiná, J. Kurchan, and L. Peliti, Phys. Rev. Lett. **96**, 120603 (2006).
[31] J. Tailleur and J. Kurchan, Nat. Phys. **3**, 203 (2007).
[32] T. Yanagita and Y. Iba, J. Stat. Mech.: Theory Exp. 2009, P02043.
[33] N. Metropolis, A. Rosenbluth, M. Rosenbluth, A. Teller, and E. Teller, J. Chem. Phys. **21**, 1087 (1953).
[34] K. Hukushima and K. Nemoto, J. Phys. Soc. Jpn. **65**, 1604 (1996).
[35] Y. Iba, Int. J. Mod. Phys. C **12**, 623 (2001).
[36] *Rugged Free Energy Landscapes: Common Computational Approaches to Spin Glasses, Structural Glasses and Biological Macromolecules*, Lecture Notes in Physics Vol. 736, edited by W. Janke (Springer, Berlin, 2008).
[37] R. Diestel, *Graph Theory* (Springer, New York, 2005).
[38] D. J. Watts and S. H. Strogatz, Nature (London) **393**, 440 (1998).
[39] P. N. McGraw and M. Menzinger, Phys. Rev. E **72**, 015101(R) (2005).
[40] We have also performed simulations with randomly selected natural frequencies, which were drawn from a distribution $g(\omega)$. The qualitative behavior was similar to that of the present model.
[41] Since diagonal elements of the adjacent matrix are chosen to be zero, the ratio is not equal to 1 at $p=1$, i.e., for all-to-all connections.